CrystEngComm

COMMUNICATION

View Article Online
View Journal | View Issue

Cite this: *CrystEngComm*, 2014, **16**, 2560

Received 12th December 2013,
Accepted 19th January 2014

DOI: 10.1039/c3ce42536c

www.rsc.org/crystengcomm

One-pot synthesis of Pd–Pt@Pd core–shell nanocrystals with enhanced electrocatalytic activity for formic acid oxidation†

Qiang Yuan,*[a] Da-Bing Huang,[a] Hong-Hui Wang,[b] Zhi-You Zhou*[b] and Qingxiao Wang[c]

Well-defined Pd–Pt@Pd core–shell nanocrystals with a Pd–Pt alloy core and a conformal Pd shell of ~2–3 nm were directly synthesized through a one-pot, aqueous solution approach without any preformed Pd or Pt seeds. These Pd–Pt@Pd core–shell nanocrystals show an enhanced electrocatalytic activity for formic acid oxidation compared with commercial Pd black.

Today, synthesis of bimetallic nanomaterials with a controlled structure, *e.g.* size, shape, core/shell, alloy and composition, has attracted increasing interest because of the superior catalytic, optic and magnetic properties of bimetallic nanomaterials relative to their monometallic counterparts.[1–5] Pd–Pt bimetallic nanocrystals are significant systems owing to their potential applications in electrocatalytic oxidation of small organic molecules (formic acid and methanol),[6,7] oxygen reduction reaction (ORR),[8] hydrogen oxidation reaction,[9] hydrogenation of aromatic hydrocarbons[10] and hydrogen storage.[11] Owing to the intrinsic physical properties of both palladium and platinum, namely, (1) both metals adopt a face-centered cubic (*fcc*) packing structure, (2) the atomic radii are within 15% of each other (1.4% for Pd and Pt, 1.37 and 1.39 Å, respectively), (3) they have similar electronegativities (2.20 and 2.28 for Pd and Pt on the Pauling electronegativity scale, respectively),[12–15] and (4) they have a very small lattice mismatch of only 0.77%, all these factors make them easily form continuous solid solutions (alloy) for all compositions through a bottom-up solution route.[16] To date, hydrothermal/solvothermal methods are mainly adopted to produce Pd and Pt bimetallic nanocrystals through coreduction of Pd and Pt precursors or a seed-mediated growth method. However, for coreduction of Pd and Pt species produced from Pd and Pt salt precursors, it is difficult to acquire core–shell nanocrystals and often results in alloy nanocrystals.[7,17–22] Pd@Pt or Pt@Pd core–shell nanocrystals[15,23–28] and Pt-on-Pd nanodendrites[8,29] were synthesized by using a two-step seed-mediated epitaxial growth method with faceted Pd or Pt nanoparticles as seeds. For example, Yang and co-workers reported the synthesis of Pt@Pd core–shell nanocrystals using a seed-mediated epitaxial growth method with 13.4 nm Pt nanocubes as seeds.[23] Similar approaches were also used to synthesize Pd@Pt or Pt@Pd core–shell nanocrystals by Xia and co-workers.[25] Beer and co-workers have demonstrated a supramolecular route for the synthesis of Pd@Pt or Pt@Pd core–shell nanoparticles, based on an anion coordinating on the surface of preformed Pd or Pt core nanoparticles.[26] Moreover, Xia's[8] and Yang's[29] groups displayed the synthesis of Pt-on-Pd bimetallic nanodendrites using sub-10 nm Pd nanoparticles as seeds. As mentioned above, Pd and Pt bimetallic heterostructures are mainly produced through a two-step seed-mediated epitaxial growth method. It seems as though it would be impossible to synthesize well-defined Pd and Pt bimetallic heterostructures (*e.g.*, core–shell structures) by coreduction of Pd and Pt species without any Pd or Pt seeds because of the intrinsic physical properties of both Pd and Pt elements. Recently, however, Yamauchi and co-workers made a significant breakthrough in the synthesis of Pt-on-Pd nanodendrite heterostructures through a one-step direct synthesis route in aqueous solution in the presence of K_2PtCl_4, Na_2PdCl_4 and Pluronic P123 with ascorbic acid (AA) as the reducing agent.[30] It greatly inspired us to explore a reasonable route for synthesis of well-defined Pd and Pt bimetallic core–shell nanocrystals without any pre-synthesized Pd or Pt seeds.

[a] *Department of Chemistry, College of Chemistry and Chemical Engineering, Guizhou University, Guizhou Province 550025, Guiyang, PR China. E-mail: sci.qyuan@gzu.edu.cn, zhouzy@xmu.edu.cn*

[b] *State Key Laboratory of Physical Chemistry of Solid Surfaces, College of Chemistry and Chemical Engineering, Xiamen University, Xiamen, 361005, PR China*

[c] *Advanced Membrane and Porous Materials Center & Imaging and Characterization Core Lab, King Abdullah University of Science and Technology, Thuwal 23955-6900, Saudi Arabia*

† Electronic supplementary information (ESI) available: Experimental details, EDS profiles, STEM images, EDS line-scanning profiles, elemental maps, TEM, and CV. See DOI: 10.1039/c3ce42536c

In this communication, for the first time, we reported a simple, one-pot, aqueous phase approach to directly produce Pd–Pt@Pd core–shell nanocrystals with a Pd–Pt alloy core and a Pd shell of ~2–3 nm without any preformed Pd or Pt seeds. Fig. 1(a) shows the representative transmission electron microscope (TEM) image of the product prepared with this "one-pot" approach. As can be seen, the product consists of a large quantity of uniform particles with a well-defined octahedral shape and the average diameter of particles is 29 nm. The high-resolution TEM (HRTEM) image of one single particle is shown in Fig. 1(b). The well-resolved, continuous fringes in the same orientation crossing through the whole particle and the corresponding Fourier transform (FT) pattern indicate that the particle is a single crystal. The spacing between two lattice fringes was measured to be 0.23 nm, closed to the (111) lattice spacing of the face-centered cubic (*fcc*) Pd/Pt. The boundary between the core and the shell is not clear because of the weak contrast of Pd and Pt under the bright-field TEM. Nevertheless, the high-angle annular dark-field scanning transmission electron microscope (HAADF-STEM) images of the product (Fig. 1c and S1 (ESI†)) show that the nanocrystals are core–shell octahedral structures with some truncation at corners and the thickness of the shell is 2–3 nm. The X-ray diffraction (XRD) pattern (Fig. 1d) of the as-synthesized product shows five peaks corresponding to (111), (200), (220), (311) and (222) of *fcc* Pd/Pt. Moreover, the energy dispersive X-ray (EDX) spectra reveal that the product is made of Pt and Pd (Fig. S2 (ESI†)).

To clarify the structure and composition of the bimetallic core–shell nanocrystals, we further combined EDX line scanning with elemental analysis mapping to analyze the core–shell nanocrystals. The positional distribution of Pd and Pt in the core–shell octahedron was revealed by EDX line-scan analysis and elemental analysis mapping. Fig. 2a–c display two line-scan EDX spectra of elemental Pd and Pt that were recorded through the center of two nanocrystals (marked by the red arrow in Fig. 2a). As can been seen,

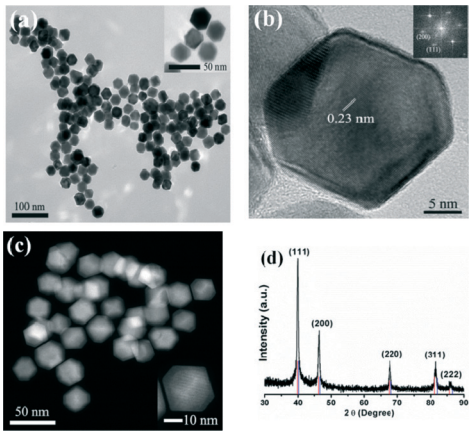

Fig. 1 TEM (a), HRTEM (b) and HADDF-STEM (c) images and XRD patterns (d) of as-synthesized Pd–Pt@Pd core–shell nanocrystals (the inset in (b) shows FT patterns of a single nanocrystal). The red and blue lines in (d) are the standard peaks for Pd (red) and Pt (blue).

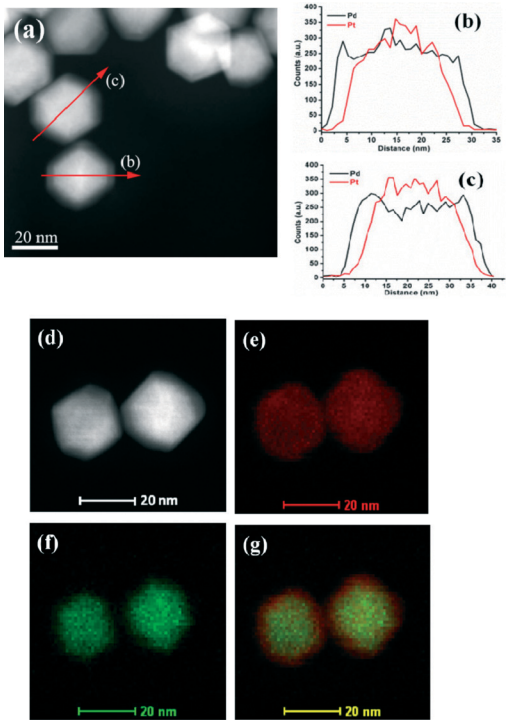

Fig. 2 HADDF-STEM image (a) and the corresponding EDX line scanning profiles (b, c) of two individual nanocrystals as indicated in (a). (d) HADDF-STEM image and the corresponding elemental maps of (e) Pd (red) and (f) Pt (green). (g) Reconstructed overlay image of the maps shown in panels (e) and (f).

there is no Pt trace at the edge of the nanocrystal in the range of 2–3 nm, while the Pd trace is very clear. It indicates that the nanocrystal is a core–shell nanostructure with a Pd shell. In the region of Pt, moreover, the signals of Pd don't obviously decrease, which is obviously different from the signals of a Pt@Pd or Pd@Pt core–shell nanocrystal.[24,25] It hints that the core of the as-synthesized core–shell nanocrystal is a Pd–Pt alloy. The suggestion was further confirmed by the elemental analysis mapping. Fig. 2d–g show the HADDF STEM images and elemental analysis maps of two as-synthesized nanocrystals. The Pd maps (Fig. 2e) have the same size and shape as the as-synthesized nanocrystals shown in Fig. 2d and the signals of Pd in the center regions of the nanocrystal are stronger than those at the edge regions. It indicates that the Pd was distributed in the whole particle. The size of the Pt maps (Fig. 2f) is obviously smaller than that of the as-synthesized nanocrystals (Fig. 2d). It indicates that there is no Pt element in the shell regions of the core–shell nanocrystals. Moreover, the overlaps of Pd and Pt maps (Fig. 2g) further confirm the above-mentioned suggestions, namely, the core–shell nanocrystals consist of a Pd shell and a Pd–Pt alloy core and the thickness of the shell is 2–3 nm.

In order to get the desired nanostructures, the appropriate capping and reducing agents are often chosen to control the morphologies of nanocrystals through tuning the reduction kinetics of precursors in the solution approach. For instance, in our previous report, high quality solid Pd–Pt nanocube

alloys were synthesized by coreduction of $PdCl_2$ and K_2PtCl_6 in the presence of KBr, sodium lauryl sulfate (SLS), and polyvinylpyrrolidone (PVP).[19] Lee and co-workers[31] described the formation of a Au@Pd core–shell nanooctahedron in the presence of cetyltrimethylammonium chloride (CTAC) in an aqueous solution of $HAuCl_4/K_2PdCl_4$. Yamauchi and co-workers[32] demonstrated the synthesis of Au@Pd@Pt core–shell nanoparticles in an aqueous solution of $HAuCl_4/Na_2PdCl_4/K_2PtCl_4$ with ascorbic acid (AA) and Pluronic F127 as reducing and capping agents, respectively. In our present work, in the preparation of Pd–Pt@Pd core–shell nanocrystals, cetyltrimethylammonium bromide (CTAB) plays an important role. To prove this suggestion, a series of control experiments were carried out. In the absence of CTAB, the product was made up of non-dispersed bulky aggregates. When an equimolar amount of CTAC replaced CTAB, no core–shell nanocrystals can be produced, and the product consists of Pd–Pt alloy nanocrystals (Fig. S3 (ESI†)). Furthermore, when an equimolar amount of NaBr replaced CTAB, the product was made up of non-dispersed irregular aggregates (Fig. S4 (ESI†)). However, in the absence of citric acid (CA), no product was acquired. These results indicate that CTAB and CA mainly act as capping and reducing agents, respectively. In addition, to get Pd–Pt@Pd core–shell nanocrystals, the molar ratio of Na_2PdCl_4 to H_2PtCl_6 is also a key factor. When decreasing the molar ratio of Na_2PdCl_4 to H_2PtCl_6 from 2 : 1 to 1 : 1, the results of elemental analysis mapping and CV in H_2SO_4 (Fig. 3) show that the product does not consist of Pd–Pt@ Pd core–shell nanocrystals but Pd–Pt alloy nanocrystals. While decreasing the molar ratio of Na_2PdCl_4 to H_2PtCl_6 to 1 : 4, the product consists of sphere-like alloy particles (Fig. 4) and no core–shell Pd–Pt@Pt nanocrystals were acquired. Furthermore, the thickness of the Pd shell can be increased simply by increasing the amount of Pd precursors. When the molar ratio of Na_2PdCl_4 to H_2PtCl_6 is 4 : 1, the thickness of the Pd shell is about 7.8 nm (Fig. S5 (ESI†)). Based on the above-mentioned experimental results, we deduce that the formation mechanism of Pd–Pt@Pd core–shell nanocrystals is mainly through the following steps: firstly, when CTAB was added in the aqueous solution, Cl^- anions in the precursors were easily replaced by Br^- anions to form harder to reduce $PdBr_4^{2-}$ and $PtBr_6^{2-}$ species ($PdCl_4^{2-}$/Pd (0.62 V *versus* RHE); $PtCl_6^{2-}$/Pt (0.74 V *versus* RHE); $PdBr_4^{2-}$/Pd (0.49 V *versus* RHE) and $PtBr_6^{2-}$/Pt (0.61 V *versus* RHE)) because Pd^{2+}/Pt^{4+} binds to Br^- more strongly than Cl^-,[31–36] then $PdBr_4^{2-}$ and $PtBr_6^{2-}$ species were reduced to form a Pd–Pt alloy with CA, and finally, the Pd shell was formed on the Pd–Pt alloy cores through epitaxial and conformal growth by reduction of the rest of the Pd^{2+} species.

The electrocatalytic activity for formic acid oxidation of as-synthesized Pd–Pt@Pd core–shell nanocrystals was tested and compared with commercial Pd black. As shown in Fig. 5a, the CV of Pd–Pt@Pd shows a similar shape with that of the commercial Pd black and is different from the CVs of Pd–Pt alloys.[7,19] It also confirms that the as-synthesized nanocrystals have a core/shell structure with a Pd shell, not an alloy structure. In the positive scanning direction, the two peaks stand for

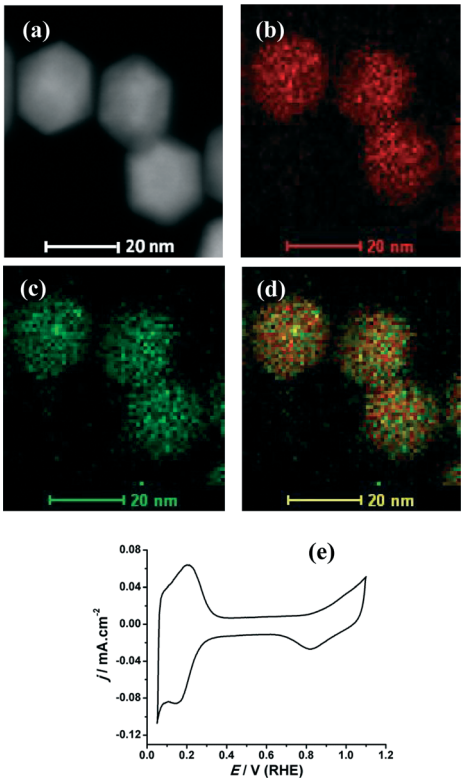

Fig. 3 HADDF-STEM image (a), the corresponding elemental maps of (b) Pd (red) and (c) Pt (green), (d) reconstructed overlay image shown in panels (b) and (c) and (e) CV in 0.1 M H_2SO_4 solution of nanocrystals synthesized with a molar ratio of Na_2PdCl_4 to H_2PtCl_6 of 1 : 1.

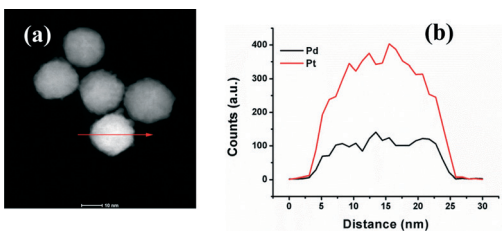

Fig. 4 HADDF-STEM image (a) and EDX line scanning profiles (b) of nanocrystals synthesized with a molar ratio of Na_2PdCl_4 to H_2PtCl_6 of 1 : 4.

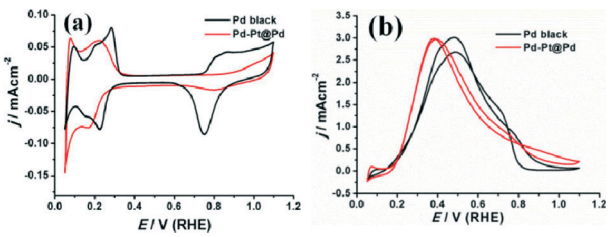

Fig. 5 The cyclic voltammetric curves (CVs) of as-synthesized Pd–Pt@Pd core–shell nanocrystals (red) and commercial Pd black (black) (a) in 0.1 M H_2SO_4 solution and (b) in 0.1 M formic acid + 0.1 M H_2SO_4 solution.

hydrogen under potential desorption (H_{upd}) and the formation of a hydroxide layer (OH_{ad}) on the surface of nanocrystals, respectively. In the negative scanning direction, the two peaks correspond to the surface reduction of nanocrystals and hydrogen adsorption, respectively. The H_{upd} and OH_{ad} peaks

of the Pd–Pt@Pd nanocrystals shift negatively and positively, respectively, as compared with those of the commercial Pd black, which may be attributed to the thin Pd shell of the Pd–Pt@Pd nanocrystals. The hydrogen adsorption/desorption electric charges calculated from CVs were used to estimate the electrochemically active surface area (ECSA) of catalysts. Fig. 5b shows the comparison of electrocatalytic properties of the Pd–Pt@Pd nanocrystals and commercial Pd black for formic acid oxidation. The current has been normalized by ECSA to yield current density (j). The two samples have a similar current density, about 3.1 mA cm^{-2}. However, the peak potential of Pd–Pt@Pd nanocrystals is much lower than that of commercial Pd black; they are 0.37 and 0.48 V, respectively. It indicates that formic acid is more easily oxidized on the surface of Pd–Pt@Pd nanocrystals than that of commercial Pd black. Moreover, when the potential is 0.3 V, the current density of Pd–Pt@Pd nanocrystals is 2.0 mA cm^{-2} and that of commercial Pd black is 1.2 mA cm^{-2}. It shows that the current density of Pd–Pt@Pd nanocrystals has an obvious enhancement. However, the stability of Pd–Pt@Pd nanocrystals is weaker than that of commercial Pd black (Fig. S6 (ESI†)).

Conclusions

In conclusion, for the first time, we have developed a simple one-pot aqueous phase approach to directly produce well-defined Pd–Pt@Pd core–shell nanocrystals with a Pd–Pt alloy core and a Pd shell of ~2–3 nm without any preformed Pd or Pt seeds. Characterization by HRTEM, FT and XRD shows that the as-synthesized Pd–Pt@Pd core–shell nanocrystals are single crystals. The electrocatalytic activity of Pd–Pt@Pd core–shell nanocrystals towards formic acid oxidation was investigated and compared with the activity of commercial Pd black. The peak potential of Pd–Pt@Pd core–shell nanocrystals decreased 0.11 V in comparison with that of commercial Pd black.

Acknowledgements

This work is supported by NSFC (21361005, 21073152 and 21373175), Fujian Provincial Department of Science and Technology (2008F3099), Foundation for the Talents by the Guizhou University (X060025) and Natural Science Foundation of Guizhou Province (20072013). We also appreciate the useful discussion with Prof. Hua Chun Zen of the National University of Singapore about this work.

Notes and references

1 C. Koenigsmann, A. C. Santulli, K. Gong, M. B. Vukmirovic, W. Zhou, E. Sutter, S. S. Wong and R. R. Adzic, *J. Am. Chem. Soc.*, 2011, **133**, 9783–9795.
2 J. W. Hong, D. Kim, Y. W. Lee, M. Kim, S. W. Kang and W. S. Han, *Angew. Chem., Int. Ed.*, 2011, **50**, 8876–8880.
3 C. J. DeSantis, A. A. Peverly, D. G. Peters and S. E. Skrabalak, *Nano Lett.*, 2011, **11**, 2164–2168.
4 M. Hu, Y. Lu, S. Zhang, S. Guo, B. Lin, M. Zhang and S. Yu, *J. Am. Chem. Soc.*, 2008, **130**, 11606–11607.
5 J. Yan, X. Zhang, T. Akita, M. Haruta and Q. Xu, *J. Am. Chem. Soc.*, 2010, **132**, 5326–5327.
6 H. Lee, S. E. Habas, G. A. Somorjai and P. D. Yang, *J. Am. Chem. Soc.*, 2008, **130**, 5406–5407.
7 Y. Liu, M. Chi, V. Mazumder, K. L. More, S. Soled, J. D. Henao and S. H. Sun, *Chem. Mater.*, 2011, **23**, 4199–4203.
8 B. Lim, M. J. Jiang, P. H. C. Camargo, E. C. Cho, J. Tao, X. M. Lu, Y. M. Zhu and Y. N. Xia, *Science*, 2009, **324**, 1302–1305.
9 H. Zhang, M. Jin, H. Liu, J. Wang, M. J. Kim, D. Yang, Z. Xie, J. Liu and Y. N. Xia, *ACS Nano*, 2011, **5**, 8212–8222.
10 Y. Yu, B. Fonfé, A. Jentys, G. L. Haller, J. A. Veen, O. Y. Gutiérrez and J. A. Lercher, *J. Catal.*, 2012, **292**, 13–25.
11 H. Kobayashi, M. Yamauchi, H. Kitagawa, Y. Kubota, K. Kato and M. Takata, *J. Am. Chem. Soc.*, 2010, **132**, 5576–5577.
12 S. Chen, P. Ferreira, W. Sheng, N. Yabuuchi, N. Allard and Y. Shao-Horn, *J. Am. Chem. Soc.*, 2008, **130**, 13818–13819.
13 W. Callister, *Materials Science and Engineerings—An Introduction*, Wiley, New York, 7th edn, 2006, p. 84.
14 F. Tao, M. Grass, Y. Zhang, D. Butcher, J. Renzas, Z. Liu, J. Chung, B. Mun, M. Salmeron and G. Somorjai, *Science*, 2008, 932–934.
15 S. I. Sanchez, W. M. Small, J. Zuo and R. G. Nuzzo, *J. Am. Chem. Soc.*, 2009, **131**, 8683–8689.
16 F. R. De Boer, R. Boom, W. C. M. Mattens, A. R. Miedama and A. K. Niessen, *Cohesion in Metals: Transition Metal Alloys*, Elsevier, Amsterdam, 1988.
17 X. Huang, H. Zhang, C. Guo, Z. Zhou and N. Zheng, *Angew. Chem., Int. Ed.*, 2009, **48**, 4808–4812.
18 B. Lim, J. G. Wang, P. H. C. Camargo, C. M. Cobley, M. J. Kim and Y. N. Xia, *Angew. Chem., Int. Ed.*, 2009, **48**, 6304–6307.
19 Q. Yuan, Z. Zhou, J. Zhuang and X. Wang, *Chem. Commun.*, 2010, **46**, 1491–1493.
20 Y. Lee, A. Ko, S. Han, H. Kim and K. Park, *Phys. Chem. Chem. Phys.*, 2011, **13**, 5569–5572.
21 A. Yin, X. Min, W. Zhu, H. Wu, Y. W. Zhang and C. H. Yan, *Chem. Commun.*, 2012, **48**, 543–545.
22 A. Yin, X. Min, Y. W. Zhang and C. H. Yan, *J. Am. Chem. Soc.*, 2011, **133**, 3816–3819.
23 S. Habas, H. Lee, V. Radmilovic, G. Somorjai and P. D. Yang, *Nat. Mater.*, 2007, **6**, 692–697.
24 B. Lim, J. Wang, P. H. C. Camargo, M. Jiang, M. J. Kim and Y. N. Xia, *Nano Lett.*, 2008, **8**, 2535–2540.
25 H. Zhang, M. Jin, J. Wang, M. J. Kim, D. Yang and Y. N. Xia, *J. Am. Chem. Soc.*, 2011, **133**, 10422–10425.
26 C. J. Serpell, J. Cookson, D. Ozkaya and P. D. Beer, *Nat. Chem.*, 2011, **3**, 478–483.
27 Y. Wang and N. Toshima, *J. Phys. Chem. B*, 1997, **101**, 5301–5306.
28 R. Choi, S. Choi, C. Choi, K. M. Nam, S. Woo, J. Park and S. W. Han, *Chem.–Eur. J.*, 2013, **19**, 8190–8198.
29 Z. M. Peng and H. Yang, *J. Am. Chem. Soc.*, 2009, **131**, 7542–7543.
30 L. Wang, Y. Nemoto and Y. Yamauchi, *J. Am. Chem. Soc.*, 2011, **133**, 9674–9677.

31 Y. Lee, M. Kim, Z. Kim and S. Han, *J. Am. Chem. Soc.*, 2009, **131**, 17036–17037.
32 L. Wang, Y. Nemoto and Y. Yamauchi, *J. Am. Chem. Soc.*, 2010, **132**, 13636–13638.
33 F. Fan, A. Attia, U. K. Sur, J. Chen, Z. Xie, J. Li, B. Ren and Z. Q. Tian, *Cryst. Growth Des.*, 2009, **9**, 2335–2340.
34 B. Veisz and Z. Király, *Langmuir*, 2003, **19**, 4817–4824.
35 Y. Borodko, L. Jones, H. Lee, H. Frei and G. Somorjai, *Langmuir*, 2009, **25**, 6665–6671.
36 M. Grzelczak, J. Pérez-Juste, B. Rodríguez-González, M. Spasova, I. Barsukov, M. Farle and L. M. Liz-Marzán, *Chem. Mater.*, 2008, **20**, 5399–5405.

